



2-25-2011

# Internal Stresses, Normal Modes, and Nonaffinity in Three-Dimensional Biopolymer Networks

E. M. Huisman

*Instituut-Lorentz*

Thomas C. Lubensky

*University of Pennsylvania*, [tom@physics.upenn.edu](mailto:tom@physics.upenn.edu)

Follow this and additional works at: [http://repository.upenn.edu/physics\\_papers](http://repository.upenn.edu/physics_papers)

 Part of the [Physics Commons](#)

## Recommended Citation

Huisman, E. M., & Lubensky, T. C. (2011). Internal Stresses, Normal Modes, and Nonaffinity in Three-Dimensional Biopolymer Networks. Retrieved from [http://repository.upenn.edu/physics\\_papers/130](http://repository.upenn.edu/physics_papers/130)

## Suggested Citation:

Huisman, E.M. and Lubensky, T.C. (2011). Internal Stresses, Normal Modes, and Nonaffinity in Three-Dimensional Biopolymer Networks. *Physical Review Letters*. **106**, 088301.

© 2011 The American Physical Society

<http://dx.doi.org/10.110/PhysRevLett.106088301>

This paper is posted at Scholarly Commons. [http://repository.upenn.edu/physics\\_papers/130](http://repository.upenn.edu/physics_papers/130)

For more information, please contact [repository@pobox.upenn.edu](mailto:repository@pobox.upenn.edu).

---

# Internal Stresses, Normal Modes, and Nonaffinity in Three-Dimensional Biopolymer Networks

## Abstract

We numerically investigate deformations and modes of networks of semiflexible biopolymers as a function of crosslink coordination number  $z$  and strength of bending and stretching energies. In equilibrium filaments are under internal stress, and the networks exhibit shear rigidity below the Maxwell isostatic point. In contrast to two-dimensional networks, ours exhibit nonaffine bending-dominated response in all rigid states, including those near the maximum of  $z = 4$  when bending energies are less than stretching ones.

## Disciplines

Physical Sciences and Mathematics | Physics

## Comments

Suggested Citation:

Huisman, E.M. and Lubensky, T.C. (2011). Internal Stresses, Normal Modes, and Nonaffinity in Three-Dimensional Biopolymer Networks. *Physical Review Letters*. **106**, 088301.

© 2011 The American Physical Society

<http://dx.doi.org/10.1103/PhysRevLett.106088301>

## Internal Stresses, Normal Modes, and Nonaffinity in Three-Dimensional Biopolymer Networks

E. M. Huisman<sup>1</sup> and T. C. Lubensky<sup>2</sup>

<sup>1</sup>*Universiteit Leiden, Instituut-Lorentz, Postbus 9506, NL-2300 RA Leiden, The Netherlands*

<sup>2</sup>*Department of Physics and Astronomy, University of Pennsylvania, Philadelphia, Pennsylvania 19104, USA*

(Received 13 August 2010; published 25 February 2011)

We numerically investigate deformations and modes of networks of semiflexible biopolymers as a function of crosslink coordination number  $z$  and strength of bending and stretching energies. In equilibrium filaments are under internal stress, and the networks exhibit shear rigidity below the Maxwell isostatic point. In contrast to two-dimensional networks, ours exhibit nonaffine bending-dominated response in all rigid states, including those near the maximum of  $z = 4$  when bending energies are less than stretching ones.

DOI: 10.1103/PhysRevLett.106.088301

PACS numbers: 82.35.Lr, 63.50.-x, 83.60.Bc, 87.16.Ka

Networks of semiflexible biopolymers (NSFP) [1–4] are important for determining and controlling the mechanical properties of eukaryotic cells. Understanding their properties, in particular, the relation between mechanical response and network architecture, has been a major goal of biophysics research. NSFPs consist of long filaments of average length  $L$  linked two at a time by crosslinks so that each is connected to at most four others [5–8]. The crosslinks we consider, which we will refer to as nodes, allow free rotations of filaments relative to each other. They divide the filaments into a series of segments, of average length  $l_c$ , that give rise to a central force between nodes determined by the force-extension curve of a semiflexible polymer. In addition, bending forces favor parallel alignment of contiguous segments on the same filament. The mechanical properties of NSFPs depend on their connectivity, parametrized by the average coordination number  $z$  of their nodes or by the ratio  $L/l_c$ , on their interaction parameters, and on their architecture.

Networks of semiflexible polymers have much in common with those that occur in network glasses [9–11]. They are both continuous random networks [12], they both have nodes with maximum coordination number 4, and they are both stabilized below the central-force rigidity threshold by bending forces, between all bonds in the latter but only between segments in the same filament in the former. Careful mode counting and study of the mode structure of network glasses [9–11] and other random systems such as jammed hard spheres [13–15] have provided fundamental insight into the physics of these systems. They have also been used in the study of two-dimensional NSFPs [16]. In this Letter, we undertake a similar study of the zero-frequency shear modulus and the mode structure of simulated three-dimensional NSFPs [17] as a function of their connectivity and interaction parameters.

If a system of nodes and links in  $d$  dimensions has zero-frequency “floppy” modes [10] besides the trivial set of rigid translations and rotations, it is mechanically unstable,

though it is often stable with respect to macroscopic stress. As Maxwell [18] showed, in an unstressed system the number of floppy modes  $N_0$  can be estimated by subtracting the number of constraints  $N_c$  from the number of degrees of freedom,  $N_0 = dN - N_c$  (neglecting the sub-extensive trivial zero modes), where  $N$  is the number of nodes. In the following we consider the forces as constraints. We define  $N_k$  as the number of nodes on filament  $k$  and  $N_F$  as the number of filaments, and in our simulations we explicitly remove all disconnected clusters and all filaments with  $N_k = 0$  and  $N_k = 1$ . Each node is shared by exactly two filaments, and  $N = \frac{1}{2} \sum N_k$ . In our system, each of the  $N_k - 1$  segments on a filament provides one constraint for a total of  $N_s = \sum_{k>1} (N_k - 1) = 2N - N_F$  compressional constraints. Because segments on a single filament that meet at a common node are not parallel in our system, each of the  $N_k - 2$  nodes on filament  $k$  not connected to a dangling end contributes a single constraint for a total of  $N_b = \sum_{k>1} (N_k - 2) = 2N - 2N_F$  bending constraints. Thus,  $N_0 = dN - N_s - N_b = 3N_F - (4 - d)N$ . We define the average coordination  $z \equiv 2N_s/N$ . Then  $N_F/N = 2 - (z/2)$ ,  $N_0 = N[2 + d - (3/2)z]$ , and the critical coordination number below which floppy modes first appear is  $z_c = (2/3)(2 + d)$ . In  $2d$ ,  $z_c = 8/3$ , and in  $3d$ ,  $z_c = 10/3$ , a value that, as expected, is greater than the value  $12/5$  in  $3d$  network glasses [10]. It is common practice to characterize NSFPs by  $L/l_c$  rather than by  $z$ . In our case, dangling ends each contribute an average of  $l_c/2$  to the length of a segment. Thus  $L/l_c$  is equal to the number of nodes per polymer,  $\sum_k N_k/N_F = 2N/N_F = (1 - \frac{1}{4}z)^{-1}$ , and  $(L/l_c)_c = 6$  in  $3d$ .

We do not represent all monomers explicitly but rather integrate out all degrees of freedom of the polymers between nodes. We use the linear approximation to the nonlinear force-extension curve of semiflexible polymers. Our Hamiltonian is thus a sum over all segment free energies and over all bending energies of pairs of segments that are connected along a filament, resulting in

$$\frac{E}{k_B T} = \sum_i \frac{l_p^2}{l_{c,i}^4} (r_i - r_{0,i})^2 + \beta \sum_{i,j} \frac{l_p}{l_{c,i} + l_{c,j}} \Theta_{i,j}^2, \quad (1)$$

where  $l_p$  is the persistence length of the filaments,  $l_{c,i}$ ,  $r_i$ , and  $r_{0,i}$  are, respectively, the polymer length, the end-to-end length, and the equilibrium end-to-end length of segment  $i$ , and  $\Theta_{i,j}$  is the angle between segment  $i$  and  $j$ .

We construct our networks via a Monte Carlo relaxation process. We start with a random, isotropic network that can be considered as a single filament that crosses itself 1000 times [17]. After a large number of Monte Carlo moves that alter the topology of the network, we cut segments of this filament, until we obtain an average filament length  $L$ . We assign a polymer length  $l_c^s$  to each segment such that the equilibrium end-to-end length of each segment is equal to the actual distance between the nodes they connect. After generation, the network is in equilibrium, but the filaments are slightly bent— $\Theta_{i,j} \neq 0$ —and, as a result, there are internal stresses in the system. For all networks, during generation we keep  $l_c = \sum_s l_c^s / N_s$ ,  $l_p$ , and  $\beta$  fixed, such that  $l_p / l_c \approx 16$  and  $\beta = 1.0$ .  $l_p$  is a measure for the relative stiffness of bending versus stretching. In order to isolate the effects of bending and stretching without altering the network structure and contour lengths, we vary  $\beta$ . We could, however, vary  $l_p$  at constant  $l_c$  to produce the same effect. Letting  $l_p \rightarrow \beta^{-1} l_p^0$ , where  $l_p^0$  is the value of  $l_p$  at  $\beta = 1$  reproduces Eq. (1) with energy measured in unit of  $\beta^2 k_B T$ . Thus with  $l_p^0 / l_c = 16$ ,  $\beta = 10.0$  coincides with  $l_p / l_c = 1.6$  and  $\beta = 0.1$  with  $l_p / l_c = 160$ . In addition we vary  $L$ —and thus the average number of nodes per filament  $L / l_c$ —by changing the number of segments we cut. Finally, we focus on an experimentally relevant parameter space, with networks with on average 4, 5, 6, 8, 12, and 20 nodes per filament or, equivalently, with coordination number  $z = 3.0, 3.2, 3.33, 3.5, 3.66, \text{ and } 3.8$ . In real-life networks, typical ratios between  $l_p$  and  $l_c$  coincide with values of  $\beta$  ranging from 0.05 (e.g., cortical actin networks [19]) to 10 (e.g., fibrin networks [5]); here we take values of  $\beta$  ranging from 0.0001 to 10. All data shown are averages over nine network realizations.

We calculate the dynamical matrix from the harmonic expansion of the energy about its force-free equilibrium state and use commercially available routines to find the eigenvalues and eigenmodes of the system, neglecting any damping effects arising, in particular, from interactions with a surrounding fluid. Figure 1 graphically represents one localized and one delocalized eigenmode.

To investigate the Maxwell mode counting in our networks, we remove the internal stresses by subtracting the zero strain angle  $\Theta_{i,j,0}$  between two segments from the actual angle  $\Theta_{i,j}$  in our Hamiltonian. We then count the number of zero modes by calculating the dimension of the null space of the dynamical matrix, and we verify the relation  $N_0 = N[5 - \frac{3}{2}z]$ . We verify the stretching relation  $N_s = \sum (N_k - 1)$  by explicitly counting the number of

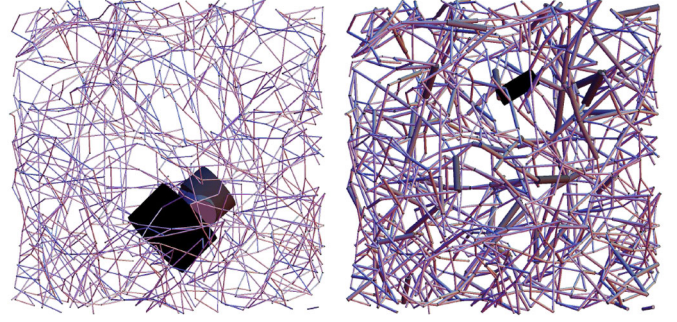


FIG. 1 (color online). Graphical representations of two eigenmodes of one our networks, left: ( $\omega = 27$ ,  $P^{-1} = 0.51$ ) and right: ( $\omega = 1.4$ ,  $P^{-1} = 0.0029$ ), where  $\omega$  is the eigenfrequency and  $P^{-1}$  is the inverse participation ratio (see the discussion of Fig. 3). All filaments in the networks are shown. The thick and dark beams indicate large deformations.

finite-frequency modes for networks with  $\beta = 0$ , and thus no bending constraints. We also verify that  $N_b = \sum_k (N_k - 2)$  by varying the number of nodes with nonzero bending modulus  $\beta$ . When internal stresses are turned back on, the floppy modes are tightened, and there are only finite-frequency modes for all  $z (\geq 3.0)$  and all  $\beta > 0$ . Also the lengthening of a single segment in the unstressed samples generates stress in a finite fraction of the segments and elevates floppy modes to finite frequency a full 10% below the Maxwell threshold. This is comparable to the rigid “stressed” state of network glasses, that exists for  $z$  just below the Maxwell threshold of 2.4 [11].

We calculate the relaxed shear modulus  $G$  for networks with and without internal stresses and for a range of  $z$  and  $\beta$  by minimizing the elastic energy after deforming the network by a small shear increment. Figure 2 summarizes our results. For all values of  $\beta$ ,  $G(z)$  is a monotonic increasing function of  $z$ , reaching its lowest but nonzero value at  $z = 3.0$ , the smallest values in our simulations. As shown by the dotted curve in Fig. 2(b), in the unstressed networks,  $G$  is zero to within the accuracy of our simulations for  $z < z_c$  and develops a nonzero value in the vicinity of the Maxwell value of  $z = z_c$ , growing approximately as a power law for  $z > z_c$ , though we cannot rule out a first-order transition. In the stressed state our data are consistent with a second-order rigidity threshold at  $z = z_p \approx 2.7 < 3.0$ , though again, we cannot rule out a first-order transition. For all  $\beta$ ,  $\log(G/\beta)$  grows linearly with  $\log(z - z_p)$ , where the slope is around 2.7 for  $\beta = 10^{-4}, 10^{-2}, \text{ and } 10^{-1}$  and then decreases with  $\beta$  to a value around 1.1 at  $\beta = 10$ . A  $\beta$ -depending slope does not surprise us, since for large  $\beta$ , we expect the deformation to be dominated by (affine) stretching of the segments, the number of which linearly increases with  $z$ , leading to a slope of 1. At small  $\beta$ , the response to shear occurs preferentially through bending modes, and  $G$  is more sensitive to changes in  $z$ , as reflected in the larger value of the slope. For the smallest values of  $\beta$ ,  $G$  becomes approximately linear in  $\beta$  for all

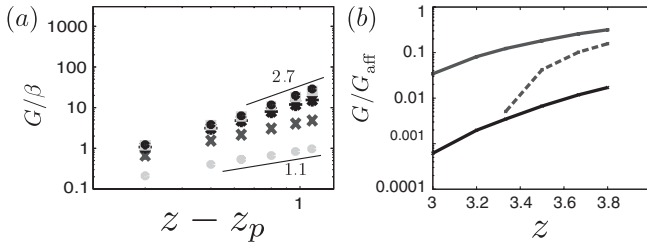


FIG. 2. (a) Double logarithmic plot of  $G/\beta$  in networks with prestress as a function of  $z - z_p$  for different values of  $\beta$ . Data points are from simulation, error bars are smaller than the size of the symbols. The slope of the data points ranges from 2.7 upper, overlapping data points for  $\beta = 0.0001$  and  $\beta = 0.001$ , 2.6 ( $\beta = 0.01$ ), 2.1 ( $\beta = 0.1$ ), 1.5 ( $\beta = 1.0$ ), and 1.1 ( $\beta = 10.0$ , lower points). A value of  $G = 1$  corresponds to an elastic modulus of  $\approx 10$  mPa for an actin network with a concentration  $f$  actin of  $\approx 0.05$  mg/ml. (b)  $G/G_{\text{aff}}$  as a function of  $z$ , for  $\beta = 1.0$  (upper curve) and  $\beta = 0.01$  (lower curve). The dotted curve shows data from unstressed network, for  $\beta = 1.0$ .

values of  $z$ , which again demonstrates that bending dominates the deformation, as is the case in glasses [20].

There are many examples of structures in which external stresses can remove floppy modes. Here we show that internal stresses can have a similar effect, reminiscent of tensegrity structures, in which rigidity can be achieved below the Maxwell threshold by stressed cables and compressed struts in carefully designed configurations [21]. In contrast to these configurations, our networks are random, and rigidity is a consequence of competition between stretching and bending rather than between stretching and compression. If the network has a structure in which filaments can support self-stress, a modified Maxwell rule  $N_0 = dN - N_c + S$ , where  $S$  is the number of states of self-stress [22] or, equivalently, the number of redundant bonds [23], applies to the stressless state. Thus, even though global Maxwell counting would indicate the contrary, biopolymer networks with internal stresses may not have floppy modes and may support shear below the stressless Maxwell rigidity threshold.

Network geometry, coordination number, and spatial dimension are all important to the determination of macroscopic elastic response. Two-dimensional lattices with  $z = 4$ , such as the kagome lattice and the  $L/l_c \rightarrow \infty$  limit of the Mikado lattice formed by the randomly depositing rods on a plane, are isostatic with respect to stretch, and they both exhibit affine response with nonzero shear and bulk moduli that are independent of  $\beta$ . The transition from nonaffine bending-dominated to nearly affine stretching-dominated response observed in diluted Mikado lattices in Refs. [6,7,24] is thus not surprising. Three-dimensional systems with  $z = 4$  are subisostatic with respect to stretch, and one might expect that bending forces are required for stabilization against shear. This is indeed the case for the  $z = 4$  diamond lattice, none of whose bond-angles are zero (i.e., all filaments are straight), whose shear modulus vanishes linearly with  $\beta$  [20]. On the other hand, a recently

constructed 3d generalization of the kagome lattice consisting of infinitely long straight filaments with crosslink coordination of exactly four provides a counterexample to this behavior [25]. Because all its filaments are straight it has a persistent triangular motif, all of its elastic moduli are nonzero when  $\beta = 0$ . As is the case in most biopolymer networks and in the diamond lattice, the filaments in our network are not straight, so we expect behavior closer to that of the diamond lattice than to that of the straight-filament 3d lattice with nonaffine bending-dominated response and a shear modulus that vanishes with  $\beta$  even in the limit  $z \rightarrow 4$ . Though our simulations do not reach sufficiently close to  $z = 4$  to unambiguously determine behavior at  $z = 4$ , they provide strong evidence that this expectation is fulfilled. Figure 2(b) shows it is highly improbable that the affine limit,  $G/G_{\text{aff}} = 1$ , is reached for small  $\beta$ . Instead, we find that  $G \propto \beta$  for the smallest values of  $\beta$  in Fig. 2(a), implying that  $G/G_{\text{aff}}$  vanishes with vanishing  $\beta$ .

We now turn to the mode structure of these networks. Figure 3 shows the density of states  $D(\omega)$  and the inverse participation ratio which provides a measure of the degree of localization of the eigenmodes [15],

$$P^{-1}(\omega) = \frac{\sum_{i=1}^N |e_{i_\omega} \cdot e_{i_\omega}|^2}{|\sum_{i=1}^N e_{i_\omega} \cdot e_{i_\omega}|^2}. \quad (2)$$

In Eq. (2),  $e_{i_\omega}$  is the polarization vector of node  $i$  in the mode  $\omega$ . The value for  $P^{-1}(\omega)$  will be 1.0 if the mode displaces one node, 0.5 if the mode displaces two nodes, and it will be  $1/N$  for the translational zero modes. The reduced frequency  $\omega$  corresponds to physical frequencies  $\tilde{\omega} \approx 10^6 \omega \text{ s}^{-1}$  for actin ( $l_p = 16 \mu\text{m}$  and  $l_c = 1 \mu\text{m}$ ) and  $\tilde{\omega} \approx 10^5 \omega \text{ s}^{-1}$  for fibrin bundles ( $l_p = 33 \mu\text{m}$  and  $l_c = 2 \mu\text{m}$ , as analyzed in [26]). These frequencies will decrease if the viscosity of the surrounding fluid is included.

Figure 3(a) shows the density of states,  $D(\omega)$  as a function of  $\log \omega$  with logarithmic binning for  $\beta = 0.0001, 0.01$ , and  $1.0$  at  $z = 3.33$ . For  $\beta = 0.01$  and  $\beta = 0.0001$ , there is a peak in  $D(\omega)$  at  $\omega \approx 2$  that corresponds to stretching modes. Its total area for  $\beta = 0.0001$  is equal to the number of stretching constraints,  $2N - N_F$  or equivalently to the number of nonvanishing modes at  $\beta = 0$ . With increasing  $z$ , the area under the right peak increases, as we would expect from the increase in the number of stretching constraints (data not shown). There is a second peak at smaller  $\omega$  that moves to the left as  $\beta$  decreases. We verified that the total area under this peak is  $N'_b = N_0 + N_b$ , where  $N_0$  is the number of zero modes of the unstressed network, and  $N_b$  is the number of bending constraints. Where possible, shear deformation will take place via these soft bending modes. As we have seen,  $G \sim \beta$  for small  $\beta$ , which implies that this is indeed the case. Again, we average over narrow bins of frequency with fixed logarithmic width to obtain  $P^{-1}(\log \omega)$ , which is plotted

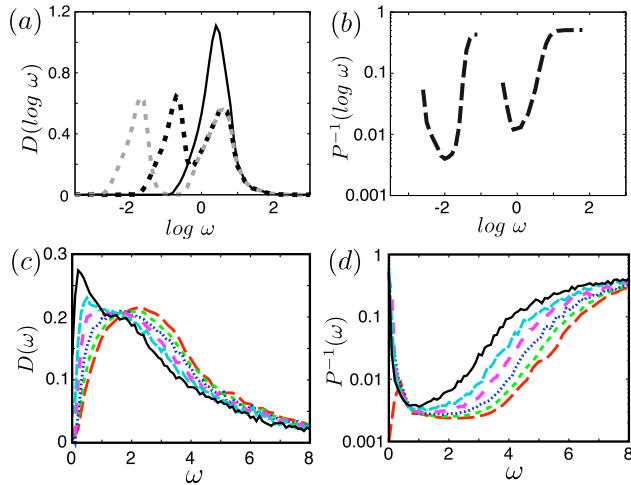


FIG. 3 (color online). (a) The logarithm of the density of states, for  $\beta = 1.0$  (solid curve),  $\beta = 0.01$  (black dotted), and  $\beta = 0.0001$  (gray dotted) for networks with  $z = 3.33$ . Note that the right peak of the latter two curves overlaps, and the left peak is shifted. (b) The inverse participation ratio for  $\beta = 0.0001$ , again for  $z = 3.33$ . (c) The density of states and (d) the inverse participation ratio as a function of  $z$ . All data shown are for networks with  $\beta = 1.0$  and (starting from the solid line)  $z = 3.0$ ,  $z = 3.2$ ,  $z = 3.33$ ,  $z = 3.5$ ,  $z = 3.66$ , and  $z = 3.8$ . Data shown are averaged over narrow bins of (the logarithm of) frequency.

in Fig. 3(b) for  $\beta = 0.0001$ . Interestingly, both bending and stretching modes can be localized and delocalized.

Figures 3(c) and 3(d) plot  $D(\omega)$  and  $P^{-1}(\omega)$  for different values of  $z$  and  $\beta = 1.0$ . The broad distribution in  $P^{-1}$  reflects the randomness in our system. Clearly the number of soft, low-frequency modes increases with decreasing  $z$ , and these modes are less extended. At low  $z$ , the filaments are less constrained, leading to an increase in soft deformation modes; in this limit, movement of a single segment will lead to a less extended deformation field. This is reflected in the increase of  $P^{-1}$  when decreasing  $z$ . We verified that the Debye scaling is approached and the frequency at which this scaling starts decreases for decreasing  $z$ . For  $z = 3.0$  and  $z = 3.2$  we do not find a peak in  $D(\omega)$  at  $\omega = 0$ , which is consistent with the given analysis that internal stresses can remove floppy modes for  $z < z_c$ .

Our results show that networks with internal stress violate stressless Maxwell counting and exhibit rigidity and no floppy modes below the Maxwell isostatic threshold. This can be relevant for *in vivo* biopolymer networks, that might have large internal stresses which increase the stiffnesses of the cells [3]. As  $\beta \rightarrow 0$ , there is a clean separation between low-frequency bending modes and high-frequency stretching modes. As is the case in most real-life biopolymer networks but contrary to that of most biopolymer networks studied analytically and in simulations, our networks consist of bent filaments. Our simulations show that it is highly improbable for this class of networks that the affine limit is reached for  $z$  approaching 4

at small  $\beta$ . Instead, the networks deform via low-frequency bending modes. Further investigation of this model, including a more thorough comparison with network glasses and a pebble-game analysis [23] to locate the critical point and to determine its order, would clearly be interesting.

It is a pleasure to acknowledge G. T. Barkema, F. C. MacKintosh, C. Storm, E. van der Giessen, and M. Thorpe for helpful discussions and comments. E. M. H. thanks P. Janmey and the University of Pennsylvania for their generous hospitality. This work is supported in part by NSF-DMR-0520020 and NSF-DMR-0804900 (T. C. L.), and by NIH-GM083272 (E. M. H.).

- [1] B. Alberts *et al.*, *Molecular Biology of the Cell* (Garland, New York, 2008), 4th ed.
- [2] E. L. Elson, *Annu. Rev. Biophys. Biophys. Chem.* **17**, 397 (1988).
- [3] K. E. Kasza *et al.*, *Curr. Opin. Cell Biol.* **19**, 101 (2007).
- [4] P. A. Janmey *et al.*, *Nature (London)* **345**, 89 (1990).
- [5] F. C. MacKintosh, J. Käs, and P. A. Janmey, *Phys. Rev. Lett.* **75**, 4425 (1995); C. Storm *et al.*, *Nature (London)* **435**, 191 (2005).
- [6] D. A. Head, A. J. Levine, and F. C. MacKintosh, *Phys. Rev. E* **68**, 061907 (2003).
- [7] J. Wilhelm and E. Frey, *Phys. Rev. Lett.* **91**, 108103 (2003).
- [8] E. M. Huisman *et al.*, *Phys. Rev. Lett.* **99**, 208103 (2007).
- [9] J. C. Phillips, *J. Non-Cryst. Solids* **43**, 37 (1981).
- [10] M. F. Thorpe, *J. Non-Cryst. Solids* **57**, 355 (1983).
- [11] M. F. Thorpe *et al.*, *J. Non-Cryst. Solids* **266–269**, 859 (2000).
- [12] W. H. Zachariasen, *J. Am. Chem. Soc.* **54**, 3841 (1932).
- [13] A. J. Liu and S. R. Nagel, *Nature (London)* **396**, 21 (1998).
- [14] L. E. Silbert, A. J. Liu, and S. R. Nagel, *Phys. Rev. Lett.* **95**, 098301 (2005).
- [15] L. E. Silbert, A. J. Liu, and S. R. Nagel, *Phys. Rev. E* **79**, 021308 (2009).
- [16] C. Heussinger and E. Frey, *Phys. Rev. E* **75**, 011917 (2007); C. Heussinger, B. Schaefer, and E. Frey, *Phys. Rev. E* **76**, 031906 (2007).
- [17] E. M. Huisman, C. Storm, and G. T. Barkema, *Phys. Rev. E* **78**, 051801 (2008).
- [18] J. C. Maxwell, *Philos. Mag.* **27**, 294 (1864).
- [19] N. Morone *et al.*, *J. Cell Biol.* **174**, 851 (2006).
- [20] H. He and M. F. Thorpe, *Phys. Rev. Lett.* **54**, 2107 (1985).
- [21] D. E. Ingber, *Sci. Am.* **278**, 48 (1998); D. Stamenovic and D. E. Ingber, *Soft Matter* **5**, 1137 (2009).
- [22] C. R. Calladine, *Int. J. Solids Struct.* **14**, 161 (1978).
- [23] D. J. Jacobs and M. F. Thorpe, *Phys. Rev. E* **53**, 3682 (1996); M. V. Chubynsky and M. F. Thorpe, *Phys. Rev. E* **76**, 041135 (2007).
- [24] D. A. Head, F. C. MacKintosh, and A. J. Levine, *Phys. Rev. E* **68**, 025101 (2003).
- [25] O. Stenull and T. C. Lubensky (network based upon kagome lattice); C. Broedersz and F. MacKintosh (“phantom” cubic lattice) (private communication).
- [26] I. K. Piechocka *et al.*, *Biophys. J.* **98**, 2281 (2010).